Submitted to

31st International Conference on High Energy Physics, ICHEP02, July 24, 2002, Amsterdam

Abstract: **978**

Parallel Session **5**

www-h1.desy.de/h1/www/publications/conf/conf_list.html

Measurement and QCD Analysis of Inclusive Deep Inelastic Scattering at High Q^2 and Large x

H1 Collaboration

Abstract

The inclusive e^+p single and double differential cross sections for neutral and charged current processes are measured with the H1 detector at HERA. The data were taken in 1999 and 2000 at a centre-of-mass energy of $\sqrt{s} \simeq 320$ GeV and correspond to an integrated luminosity of $65.2\ \mathrm{pb}^{-1}$. The cross sections are measured in the range of four-momentum transfer squared, Q^2, between 100 and 30 000 GeV^2, and Bjorken x between 0.0013 and 0.65. The new measurements are found to be consistent with previous data and are well described by next-to-leading order QCD fits in the framework of the Standard Model. Flavour separated parton densities are extracted. The neutral current analysis is extended to small energies of the scattered electron and therefore to higher values of inelasticity y allowing a determination of the longitudinal structure function F_L at high Q^2 ($110 - 700$ GeV^2).

1 Introduction

In 1992 the HERA accelerator began operation colliding lepton–proton beams within the H1 and ZEUS experiments. Both experiments have since analysed over $100\ \mathrm{pb}^{-1}$ of luminosity per experiment. The phase space covered by HERA inclusive deep inelastic scattering (DIS) cross section measurements ranges from small Bjorken x, to the electroweak (EW) regime of the Standard Model where the four-momentum transfer squared, $Q^2 \sim 10\,000$ GeV^2 is similar to the squared masses of the EW boson propagators. At these high Q^2 values the measurements provide an insight into the partonic structure of matter and the dynamics of strong interactions, as described by quantum chromodynamics (QCD), at the smallest distance scales. QCD, formulated in the context of perturbative evolution, provides an excellent predictive tool with which to compare the data. Any deviations from this may be due to exotic phenomena beyond the Standard Model.

Both neutral current (NC) interactions, $ep \rightarrow eX$ via γ or Z^0 exchange, and charged current (CC) interactions, $ep \rightarrow \nu X$ via W exchange, can be observed at HERA yielding complementary information on the QCD and EW parts of the Standard Model. The cross sections are defined in terms of three kinematic variables Q^2, x, and y, where y quantifies the inelasticity of the interaction. The kinematic variables are related via $Q^2 = sxy$, where $\sqrt{s}$ is the ep centre-of-mass energy.

Measurements of the NC and CC cross sections in e^+p scattering have been made by H1 and ZEUS based on $\simeq 40$ pb^{-1} data sets between 1994 to 1997 [1,2] when the ep centre-of-mass energy $\sqrt{s}$ was about 300 GeV. Here, new e^+p NC and CC cross section measurements, based on data taken at a centre-of-mass energy of 320 GeV in 1999 and 2000, are presented with increased precision using a luminosity of 65.2 pb^{-1}. The data provide the most accurate neutral and charged current cross sections measured by H1 at high Q^2 based on the first phase of HERA operation.

The accuracy and kinematic coverage of the H1 neutral and charged current cross section data enable dedicated QCD analyses which both test the prediction of logarithmic scaling violations over four orders of magnitude in Q^2 and unfold parton distributions. The inclusive cross sections are principally sensitive to the up and down quark and anti-quark distributions. This is used in a novel, next-to-leading order (NLO) QCD analysis of the H1 data which is also extended to include the accurate proton and deuteron data from the BCDMS muon scattering experiment [3]. The fit parameter space is carefully narrowed using theoretical constraints adapted to the new ansatz and the experimental and phenomenological uncertainties are systematically approached. This leads to a description of the complete set of NC and CC data as well as to new determinations of the parton distribution functions (PDFs) and their uncertainties.

Finally the NC analysis is extended to high y for $800 > Q^2 > 100$ GeV^2. This extension of the kinematic range allows a determination of the longitudinal structure function, $F_L(x, Q^2)$, to be made at high Q^2. This analysis is performed on both the $99-00$ e^+p data and the e^-p data set taken in 1998 and 1999 with a luminosity of 16.4 pb^{-1}. The extended e^-p analysis and F_L extraction was not been reported on in [4].

2 Neutral and Charged Current Cross Sections

After correction for QED radiative effects, the NC cross section for the process $e^{\pm}p \rightarrow e^{\pm}X$ with unpolarised beams and corrected is given by

$$\frac{\mathrm{d}^2\sigma^{\pm}_{NC}}{\mathrm{d}x\,\mathrm{d}Q^2} = \frac{2\pi\alpha^2}{xQ^4}\left[Y_+\tilde{F}_2 \mp Y_- x\tilde{F}_3 - y^2\tilde{F}_{\scriptscriptstyle L}\right](1+\Delta^{weak}_{NC}) \ , \tag{1}$$

where $\alpha \equiv \alpha(Q^2=0)$ is the fine structure constant. The Δ^{weak}_{NC} corrections are defined in [6] with the Fermi coupling constant, G_F, and the Z boson mass, M_Z, as the other main electroweak inputs. The weak corrections, are typically less than 1% and have not been applied to the measured cross sections. The helicity dependences of the electroweak interactions are contained in $Y_{\pm} \equiv 1 \pm (1-y)^2$. The generalised structure functions $\tilde{F}_2$ and $x\tilde{F}_3$ can be decomposed as [7]

$$\tilde{F}_2 \equiv \ F_2 \ - v_e \frac{\kappa_w Q^2}{(Q^2+M_Z^2)} \ F_2^{\gamma Z} + (v_e^2+a_e^2)\left(\frac{\kappa_w Q^2}{Q^2+M_Z^2}\right)^2 F_2^Z \tag{2}$$

$$x\tilde{F}_3 \equiv \ - a_e \frac{\kappa_w Q^2}{(Q^2+M_Z^2)} xF_3^{\gamma Z} + \ (2v_e a_e)\left(\frac{\kappa_w Q^2}{Q^2+M_Z^2}\right)^2 xF_3^Z, \tag{3}$$

where $\kappa_w^{-1} = 4\frac{M_W^2}{M_Z^2}(1-\frac{M_W^2}{M_Z^2})$ in the on-mass-shell scheme [8] and M_W is defined in terms of the electroweak inputs. The quantities v_e and a_e are the vector and axial couplings of the electron to the Z^0 [8]. The electromagnetic structure function F_2 originates from photon exchange only. The functions F_2^Z and xF_3^Z are the contributions to $\tilde{F}_2$ and $x\tilde{F}_3$ from Z^0 exchange and the functions $F_2^{\gamma Z}$ and $xF_3^{\gamma Z}$ are the contributions from γZ interference. The longitudinal structure function $\tilde{F}_{\scriptscriptstyle L}$ may be decomposed in a manner similar to $\tilde{F}_2$. Its contribution is significant only at high y.

Over most of the kinematic domain at HERA the dominant contribution to the cross section comes from the electromagnetic structure function F_2. Only at large values of Q^2 do the contributions due to the Z^0 boson become important. For longitudinally unpolarised lepton beams $\tilde{F}_2$ is the same for electron and for positron scattering, while the $x\tilde{F}_3$ contribution changes sign as can be seen in eq. 1.

In the quark parton model (QPM) the structure functions F_2, $F_2^{\gamma Z}$ and F_2^Z are related to the sum of the quark and anti-quark densities

$$[F_2, F_2^{\gamma Z}, F_2^Z] = x\sum_q [e_q^2, 2e_q v_q, v_q^2+a_q^2]\{q+\bar{q}\} \tag{4}$$

and the structure functions $xF_3^{\gamma Z}$ and xF_3^Z to their difference which determines the valence quark distributions, u_v and d_v

$$[xF_3^{\gamma Z}, xF_3^Z] = x\sum_q [2e_q a_q, 2v_q a_q]\{q-\bar{q}\} = x\sum_q [2e_q a_q, 2v_q a_q] q_v \ . \tag{5}$$

The functions $q(x,Q^2)$ and $\bar{q}(x,Q^2)$ are the PDFs for quarks and anti-quarks, e_q is the charge of quark q in units of the electron charge and v_q and a_q are the vector and axial-vector weak coupling constants of the quarks.

For CC interactions the cross section corrected for QED radiative effects may be expressed as

$$\frac{\mathrm{d}^2\sigma^{\pm}_{\mathrm{CC}}}{\mathrm{d}x\;\mathrm{d}Q^2} = \frac{G_F^2}{2\pi x}\left[\frac{M_W^2}{(Q^2+M_W^2)^2}\right]\,\phi^{\pm}_{\mathrm{CC}}\,(1+\Delta^{weak}_{CC}) \tag{6}$$

$$\text{with} \qquad \phi^{\pm}_{\mathrm{CC}} = \frac{1}{2}(Y_+W_2^{\pm} \mp Y_-xW_3^{\pm} - y^2W_L^{\pm}), \tag{7}$$

where Δ^{weak}_{CC} represents the CC weak radiative corrections. The CC structure functions $W_L^{\pm}$, $W_2^{\pm}$, and $xW_3^{\pm}$ are defined in a similar manner as the NC structure functions. In the QPM (where $W_L^{\pm} \equiv 0$) they may be interpreted as sums and differences of quark and anti-quark densities and are given by

$$W_2^+ = 2x(\bar{U}+D)\;,\;\; xW_3^+ = 2x(\bar{U}-D)\;,\;\; W_2^- = 2x(U+\bar{D})\;,\;\; xW_3^- = 2x(U-\bar{D})\;. \tag{8}$$

Here U represents the sum of up-type, and D the sum of down-type quark densities and includes the electroweak couplings (cf. section 4.1).

For the presentation of the subsequent measurements it is convenient to define the NC and CC "reduced cross sections" as

$$\tilde{\sigma}_{NC}(x,Q^2) \equiv \frac{1}{Y_+}\,\frac{Q^4\,x}{2\pi\alpha^2}\,\frac{\mathrm{d}^2\sigma_{NC}}{\mathrm{d}x\mathrm{d}Q^2}, \quad \tilde{\sigma}_{CC}(x,Q^2) \equiv \frac{2\pi x}{G_F^2}\left(\frac{M_W^2+Q^2}{M_W^2}\right)^2\frac{\mathrm{d}^2\sigma_{CC}}{\mathrm{d}x\mathrm{d}Q^2}. \tag{9}$$

3 Experimental Technique

3.1 H1 Apparatus and Trigger

The co-ordinate system of H1 is defined such that the positive z axis is in the direction of the outgoing proton beam (forward direction). The polar angle θ is then defined with respect to this axis. The detector components most relevant to this analysis are the Liquid Argon (LAr) calorimeter, which measures the positions and energies of particles over the range $4^\circ < \theta < 154^\circ$, a lead-fibre calorimeter (SPACAL) covering the range $153^\circ < \theta < 177^\circ$, the PLUG calorimeter covering the range $0.7^\circ < \theta < 3.3^\circ$, and the inner tracking detectors which measure the angles and momenta of charged particles over the range $7^\circ < \theta < 165^\circ$. In the central region, $25^\circ \gtrsim \theta \gtrsim 165^\circ$, the central jet chamber (CJC) is supplemented by two z drift chambers to improve the θ measurement of the tracks in the CJC. The forward tracking detector, $\theta \lesssim 30^\circ$, is used to determine the vertex of events with no tracks in the CJC.

The ep luminosity is determined by measuring the QED bremsstrahlung event rate $ep \rightarrow ep\gamma$ in the photon tagger located at $z = -103$m. An electron tagger is placed at $z = -33$m adjacent to the beam-pipe. It is used to check the luminosity measurement and to provide information on $ep \rightarrow eX$ events at very low Q^2 (photoproduction) where the electron scatters through a small angle ($\pi - \theta < 5$ mrad). A full description of the H1 detector can be found in [9] and [10].

NC events are triggered mainly using information from the LAr calorimeter. The trigger requires an electromagnetic trigger "tower" pointing to the vertex. For electrons with energy above 11 GeV this is 100% efficient. At lower energies the triggers based on LAr information are supplemented by using additional information from the tracking detectors. In 1998 the LAr calorimeter electronics were upgraded in order to trigger on scattered leptons as low as 6 GeV, the minimum value considered in this analysis. This gives access to the high y kinematic region. For electron energies of 6 GeV6 GeV, the combined trigger efficiency is 96% for the e^+p data set, and 90% for the earlier e^-p data set.

The characteristic feature of CC events is a large missing transverse momentum, P_T^{miss}, which is identified at the trigger level using the LAr calorimeter vector sum of trigger towers. At low P_T^{miss} the efficiency is enhanced by use of an additional trigger requiring hadronic energy pointing to the event vertex in combination with track information from the inner tracking chambers. For the minimum P_T^{miss} considered in the analysis of 12 GeV the efficiency is 60%, rising to 90% for P_T^{miss} of 25 GeV.

3.2 Simulation Programs

In order to determine acceptance corrections DIS processes are generated using the DJANGO [11] Monte Carlo (MC) simulation program which is based on HERACLES [12] for the electroweak interaction and on LEPTO [13], using the colour dipole model as implemented in ARIADNE [14], to generate the QCD dynamics. The JETSET program is to simulate the hadronisation process [15]. The simulated events are produced with PDFs from an NLO QCD fit (H1 97 PDF Fit) which includes previous H1 e^+p data and is detailed in [1].

The detector response to events produced by the various generation programs is simulated in detail using a program based on GEANT [16]. These simulated events are then subjected to the same reconstruction and analysis chain as the real data.

The dominant ep background contribution to deep inelastic scattering processes is due to photoproduction (γp) processes. These are simulated using the PYTHIA [17] generator with leading order parton distribution functions for the proton and photon taken from [18]. Further background from QED-Compton processes, lepton pair production via two photon interactions, prompt photon production, and heavy gauge boson ($W^{\pm}, Z^0$) production are included in the background simulation. Non-ep backgrounds are negligible. Further details are given in [1].

3.3 Cross Section Measurement Procedure

Inelastic ep interactions are required to have a vertex within ± 35 cm of its nominal z position. High Q^2 neutral current events are selected by requiring that the event has a compact and isolated energy deposition (cluster) in the electromagnetic part of the LAr calorimeter. The scattered electron is identified as the cluster of highest transverse momentum. In the central detector region, $\theta > 40^\circ$, the cluster has to be associated with a track measured in the inner tracking chambers. Energy-momentum conservation requires the variable $E - P_z$ summed over all final state particles to be approximately equal to twice the initial electron beam energy. Restricting $E - P_z$ to be greater than 35 GeV considerably reduces the photoproduction background and the radiative corrections in which the scattered electron or bremsstrahlung photon escape undetected in the electron beam direction. In order to further suppress the photoproduction background, which increases with y, cuts are applied on $y_e = 1 - \frac{E_e'}{E_e} \sin^2 \theta_e/2$. The restriction is $y_e < 0.63$ for $Q^2 < 890$ GeV^2 and $y_e < 0.90$ for $Q^2 > 890$ GeV^2, which defines the kinematic region[1] of the *nominal analysis*.

Based on the recent upgrade of LAr electronics the neutral current analysis is extended to lower energies of the scattered electron, $E'_e > 6$ GeV, giving access to the high y region $0.63 < y_e < 0.90$ for $90 < Q^2 < 890$ GeV^2. This defines the kinematic region of the *high-y analysis*. At low energies of the scattered electron the photoproduction background, where $\pi^0 \rightarrow \gamma\gamma$ decays give rise to fake electron candidates, plays an increasingly important role . Part of this background is suppressed by requiring a well measured track linked to the calorimeter cluster. The track is further required to have the same charge as the beam lepton. Finally, the remaining background is determined directly from the data by identifying fake leptons with the wrong charge. This background is statistically subtracted from the correctly charged sample. The charge symmetry between fake lepton candidates is determined using the e^+p and e^-p data sets and is measured to be 0.99 ± 0.07. Further details are given in [20, 21].

The NC kinematics in the nominal analysis are reconstructed using the $e\Sigma$ method [22] which has the best resolution and least sensitivity to QED radiative corrections over the accessible phase space. In the *high-y analysis* the electron reconstruction method is used to reconstruct the event kinematics using only the measured energy and angle of the scattered electron. This is the most precise method at high y.

The selection of charged current events requires a large missing transverse momentum, $P_T^{miss} \geq 12$ GeV, assumed to be carried by an unseen neutrino. In addition the event must have a reconstructed vertex within ± 35 cm of its nominal position. The kinematic variables y_h and Q_h^2 are determined using the hadron kinematic reconstruction method [25]. In order to restrict the measurement to a region with good kinematic resolution the events are required to have $y_h < 0.85$ and $P_{T,h} > 12$ GeV. The measurement is restricted to the region where the trigger efficiency is acceptable by demanding $y_h > 0.03$. The CC trigger efficiency is determined using NC events in which all information associated to the scattered electron is suppressed. This method gives a precise measure of the efficiency which is found to be 79% at $Q^2 = 300\,\mathrm{GeV}^2$ and reaches 98% at $Q^2 = 3000\,\mathrm{GeV}^2$. The ep background is dominantly due to photoproduction events and is suppressed as discussed in [4]. The residual ep background is negligible for most of the measured kinematic domain, though it reaches 15% at the lowest Q^2 and the highest y. This contribution is subtracted statistically from the CC data sample with a systematic uncertainty of 30% of the subtracted events. The non-ep background is rejected using the same method as in [1]. For further details see [23, 24].

For both the NC and CC analyses the selected events are corrected for detector acceptance and migrations using the simulation and converted to bin centred cross sections using the prediction from the H1 97 PDF Fit [1].

The "QED radiative corrections" are defined in [1] and were calculated using the program HERACLES [12] as implemented in DJANGO [11] and verified with the numerical analysis program HECTOR [26].

The uncertainties on the measurement lead to systematic errors on the cross sections, which can be split into bin–to–bin correlated and uncorrelated parts. All the correlated systematic

[1] At $Q^2 = 90$ GeV^2 $y = 0.63$ corresponds to $E'_e = 11$ GeV.

errors are found to be symmetric to a good approximation. Full details about the origin of the correlated and the uncorrelated systematic errors of the NC and CC cross section measurements can be found in [1, 20, 21, 24, 27].

The measurements of high Q^2 e^+p cross sections from different running periods are combined to provide a convenient summary of the first stage of HERA operation. This combination improves the statistical precision which is the dominant error source over the full Q^2 range for the CC cross sections and for $Q^2 \gtrsim 1000$ GeV^2 for the NC cross sections. For the purpose of combination the systematic errors are assumed to be fully correlated. The combined data correspond to a luminosity of 100.8 pb^{-1}.

4 QCD Analysis

The cross section data presented here cover a huge range in momentum transfer squared, Q^2, and Bjorken x. Combined with the low Q^2 neutral current data [28], recently published by the H1 Collaboration, $e^{\pm}p$ data on structure functions of much increased accuracy are now available which allow the predictions of perturbative QCD to be tested over four orders of magnitude in Q^2, from about 1 GeV^2 to above 10^4 GeV^2 , and x, from below 10^{-4} to 0.65. The joint measurement of neutral and charged current scattering cross sections provides sensitivity to different quark flavour distributions and the gluon distribution, $xg(x, Q^2)$. This is used to determine the sum of up, anti-up, down and anti-down quark distributions (xU , $x\bar{U}$, xD , $x\bar{D}$) and to unfold the valence-quark distributions, u_v and d_v.

With the current beam energies the HERA collider data do not access the medium Q^2, large x region of deep inelastic scattering. Complementary information on quark distributions is provided by lepton-deuteron scattering data which are not yet available from HERA. Therefore in the subsequent analysis the H1 data are also combined with the precise BCDMS muon-proton and muon-deuteron scattering data, and the results are compared with the analysis of the H1 data alone.

4.1 Ansatz

Traditionally, QCD analyses of inclusive deep inelastic cross-section data use parameterisations of the valence-quark distributions and of a sea-quark distribution imposing additional assumptions on the flavour decomposition of the sea. The neutral and charged current cross section data presented here, however, are sensitive to four combinations of up-type and down-type quark distributions which for Q^2 less than the bottom quark production threshold are written as:

$$\begin{aligned} U &= u + c \\ \bar{U} &= \bar{u} + \bar{c} \\ D &= d + s \\ \bar{D} &= \bar{d} + \bar{s}. \end{aligned} \tag{10}$$

This ansatz weakens the influence of necessary assumptions on the flavour decomposition of the sea in the fit. The valence-quark distributions are obtained according to

$$u_v = U - \bar{U}, \quad d_v = D - \bar{D} \tag{11}$$

and are not fitted directly.

The charged current cross sections, eq. 6, are superpositions of the distributions given in eq.10 according to

$$\phi^+_{CC} = x\bar{U} + (1-y)^2 xD, \quad \phi^-_{CC} = xU + (1-y)^2 x\bar{D} \tag{12}$$

with the helicity determined y dependence. The neutral current cross section is dominated by the structure function F_2 which can be written as

$$F_2 = \frac{4}{9} \cdot (xU + x\bar{U}) + \frac{1}{9} \cdot (xD + x\bar{D}). \tag{13}$$

In the high Q^2 neutral current data complementary sensitivity is obtained from the interference structure function $xF_3^{\gamma Z} \propto x[2(U - \bar{U}) + (D - \bar{D})]$ but still higher luminosity is required to exploit the xF_3 function for a dedicated determination of the valence quarks. With an extra assumption on the $\bar{u}$ and $\bar{d}$ quark distributions, the $xU,\ x\bar{U},\ xD,\ x\bar{D}$ and xg distributions may be simultaneously determined using H1 NC and CC data alone. This assumption may be relaxed if deuteron data are additionally used in the fit.

The isoscalar nucleon structure function F_2^N is determined by the singlet combination of parton distributions and a small contribution from the difference of strange and charm quark distributions, i.e.

$$F_2^N = \frac{5}{18} \cdot x(U + \bar{U} + D + \bar{D}) + \frac{1}{6} \cdot x(c + \bar{c} - s - \bar{s}). \tag{14}$$

The nucleon data are obtained from the muon-deuteron cross sections measured by the BCDMS collaboration, for $x \geq 0.01$, and nuclear corrections are applied following [29].

Experimental results are used to determine the fractions of charm [30, 31] and strange [32] quarks. The present QCD analysis is rather insensitive to their actual values since in the fit to the H1 and BCDMS data c and s explicitly occur only as small corrections to F_2^N.

The analysis is performed in the $\overline{MS}$ renormalisation scheme using the QCD evolution equations [33] in NLO [34]. The structure function formulae given here are thus replaced by integral convolutions of coefficient functions and PDFs. An approach is used whereby all quarks are taken to be massless including the charm and bottom quarks which provides an adequate description of the parton densities, in the high Q^2 kinematic range of the data presented here. The bottom quark density, xb, is evolved assuming that $xb(x, Q^2) = 0$ for $Q^2 < m_b^2$ GeV^2 where m_b is the bottom quark mass.

Fits are performed to the measured cross sections calculating the longitudinal structure functions to order α_s^2 and assuming the strong coupling constant to be equal to $\alpha_s(M_Z^2) = 0.1185$ [8]. The analysis uses an x space program developed inside the H1 collaboration [35], with cross checks performed using an independent program [36]. In the fit procedure, a χ^2 function is minimised which is defined in [28]. The minimisation takes into account correlations of data points caused by systematic uncertainties allowing the error parameters, including the relative normalisation of the various data sets, to be determined by the fit.

4.2 Parameterisations

The initial parton distributions, i.e. $xP = xg,\ xU,\ xD,\ x\bar{U},\ x\bar{D}$, are parameterised at $Q^2 = Q_0^2$ in the following general form

$$xP(x) = A_q x^{B_q}(1-x)^{C_q}[1 + E_q x + D_q\sqrt{x} + F_q x^2]. \tag{15}$$

A QCD analysis requires a choice to be made for Q_0^2, the initial scale, and Q^2_{min}, the minimum Q^2 of the data considered in the analysis. Variations of both Q_0^2 and Q^2_{min} are studied. As in [28] the Q_0^2 is chosen to be 4 GeV^2, and data are included for $Q^2 \geq 3.5$ GeV^2. Reasonable variations of these choices, see table 2, are considered as part of the model uncertainties of the parton distributions determined.

The general ansatz, eq. 15, represents an overparameterisation of the description of the data considered here. This is clear both from the saturation behaviour of the χ^2 function and also from fit instabilities occasionally observed. Moreover, the choice of parameters depends on the data sets included in the fit. The H1 data can be fitted with less parameters than the combined H1 and BCDMS data due to the precise BCDMS proton and deuteron data in the large x region where the cross section variations with x are particularly strong.

Careful consideration of the parameter space leads to the following set of parameterisations in the fit to the H1 and BCDMS data

$$\begin{aligned}
xg(x) &= A_G x^{B_G}(1-x)^{C_G} \cdot [1 + E_G x + D_G\sqrt{x}] \\
xU(x) &= A_U x^{B_U}(1-x)^{C_U} \cdot [1 + E_U x + D_U\sqrt{x} + F_U x^2] \\
xD(x) &= A_D x^{B_D}(1-x)^{C_D} \cdot [1 + E_D x + D_D\sqrt{x}] \\
x\bar{U}(x) &= A_{\bar{U}} x^{B_{\bar{U}}}(1-x)^{C_{\bar{U}}} \cdot [1 + E_{\bar{U}} x] \\
x\bar{D}(x) &= A_{\bar{D}} x^{B_{\bar{D}}}(1-x)^{C_{\bar{D}}}\ .
\end{aligned} \tag{16}$$

The variations in the number of parameters for the different parton distributions are broadly in accord with expectation. The gluon distribution is not sensitive to a high x parameter, $F_G x^2$, since at large x the scaling violations are due to gluon bremsstrahlung, i.e. independent of the gluon distribution. The U and D distributions require more parameters than the anti-quark distributions $\bar{U}$ and $\bar{D}$ because the former are a superposition of valence and sea quarks, in contrast to the latter. Due to the different electric charges, $e_u^2 = 4e_d^2$, and the y dependence of the charged current cross section, the data are much more sensitive to the up quark than to the down quark distributions. Thus less parameters are needed for D than for U. The specific choice of these parameterisations is obtained from saturation of the χ^2: an additional parameter D, E, or F is considered only when its introduction improves the χ^2 by more than one unit. Furthermore solutions are excluded which yield unphysical behaviour, e.g. negative cross sections.

A number of relations between parameters can be introduced naturally in the ansatz. At low x the valence quark distributions are expected to vanish. Thus the low x parameters A_q and B_q are required to be the same for $U,\ \bar{U}$ and for $D,\ \bar{D}$ as the sea-quark and the anti-quark densities can be assumed to be equal. In the absence of deuteron data from HERA there is no distinction possible of the rise towards low x between U and D. Thus the corresponding parameters B and

D are required to be equal, i.e. $B_U = B_D = B_q$ and $D_U = D_D = D_q$. Further contraints are the conventional momentum sum rule and the valence quark counting rules. The total number of free parameters of the five parton distributions is thus equal to 13 in the fit to the H1 and BCDMS data. In the fit to the H1 data alone inclusion of the parameter D_q does not improve the χ^2 and it is omitted from the fit.

The present fit differs from traditional QCD analyses which directly parameterise either the difference $(\bar{d} - \bar{u})$ [37] or the ratio $\bar{d}/\bar{u}$ [38]. The functional forms in these ansatzes are chosen to require $(\bar{d} - \bar{u}) \rightarrow 0$ when $x \rightarrow 0$. This behaviour can be imposed to the current fit assuming that $x\bar{c}$ and $x\bar{s}$, at the starting scale of $Q_0^2 = 4$ GeV^2, can be expressed as fractions f_s and f_c of the $\bar{U}$ and $\bar{D}$ distributions, respectively. In the low x limit the ratio $\bar{d}/\bar{u}$ can then be expressed in terms of the parton distribution parameters as

$$\bar{d}/\bar{u} = \frac{1 - f_s}{1 - f_c} \frac{A_{\bar{D}}}{A_{\bar{U}}} x^{(B_{\bar{D}} - B_{\bar{U}})} \tag{17}$$

The condition $\bar{d}/\bar{u} \rightarrow 1$ as $x \rightarrow 0$ is imposed with the constraint $A_{\bar{U}} = A_{\bar{D}} \cdot (1 - f_s)/(1 - f_c)$, as well as requiring $B_{\bar{D}} = B_{\bar{U}}$.

4.3 Fit Results

The fit to the H1 and BCDMS data, termed "Preliminary H1 2002 PDF Fit", uses the data sets as specified in table 1. The total χ^2 per degree of freedom (ndf) in this fit is $917/(1014 - 13) = 0.92$. The initial parton distributions are shown in fig. 1. The inner error band describes the experimental uncertainty while the outer band represents the experimental and the model uncertainties added in quadrature. The solid line is the result of the fit to the H1 data alone, which gives a χ^2/ndf$= 548/(621 - 11) = 0.90$.

experiment	x_{min}	x_{max}	Q^2_{min} (GeV^2)	Q^2_{max} (GeV^2)	$\delta\mathcal{L}$ (%)	ref.	comment
H1 min bias $96-97$	0.00008	0.02	3.5	12	1.8	[28]	e^+p $\sqrt{s} \simeq 300$ GeV
H1 low Q^2 $96-97$	0.000161	0.20	12	150	1.8	[28]	e^+p $\sqrt{s} \simeq 300$ GeV
H1 NC $94-97$	0.0032	0.65	150	30 000	1.5	[1]	e^+p $\sqrt{s} \simeq 300$ GeV
H1 CC $94-97$	0.013	0.40	300	15 000	1.5	[1]	e^+p $\sqrt{s} \simeq 300$ GeV
H1 NC $98-99$	0.0032	0.65	150	30 000	1.8	[4]	e^-p $\sqrt{s} \simeq 320$ GeV
H1 CC $98-99$	0.013	0.40	300	15 000	1.8	[4]	e^-p $\sqrt{s} \simeq 320$ GeV
H1 NC $99-00$	0.0032	0.65	150	30 000	1.5	this rep.	e^+p $\sqrt{s} \simeq 320$ GeV; incl. *high-y anal.*
H1 CC $99-00$	0.013	0.40	300	15 000	1.5	this rep.	e^+p $\sqrt{s} \simeq 320$ GeV
H1 NC $98-99$	0.00131	0.0105	100	800	1.5	this rep.	e^-p $\sqrt{s} \simeq 320$ GeV; *high-y analysis*
BCDMS-p	0.07	0.65	7.5	230	3.0	[3]	μp; require $y_\mu > 0.3$ & $x < 0.7$
BCDMS-D	0.07	0.65	7.5	230	3.0	[3]	μD; require $y_\mu > 0.3$ & $x < 0.7$

Table 1: *Table of data sets used in the QCD fit to the H1 ep and the BCDMS μ-proton and μ-Deuteron scattering data. As for the previous H1 QCD analysis [28], the original BCDMS data are used imposing the constraint $y_\mu > 0.3$. The normalisation uncertainties of each data set ($\delta\mathcal{L}$) are given as well as the kinematic ranges in x and Q^2.*

The experimental accuracy of the initial distributions is of the order of a few percent at small x. The gluon distribution is consistent with the distribution obtained previously if the effect of the different heavy flavour treatment is taken into account, see [28].

The parameters of this analysis are specified in table 2. The model uncertainties are determined in a similar manner to [28], and the sources of uncertainty are specified in table 2. Within the considered functional form, see eq. 15, the parameterisation given in eq. 16 is found uniquely. Possible variations within the $\Delta\chi^2 \simeq 1$ region of the parameter space do not lead to noticeably different distributions. Thus no account is made for a parameterisation uncertainty in this analysis. A completely different ansatz, however, may well lead to different initial distributions as seen, for example, in the complicated shape of xg chosen in [37]. The DGLAP evolution mechanism equalises such possible initial differences to a remarkable extent in the high Q^2 region to which the data presented here belong.

source of uncertainty	central value	variation
Q^2_{min},GeV^2	3.5	$2.0 - 5.0$
Q^2_0,GeV^2	4.0	$2.0 - 6.0$
$\alpha_s(M_Z^2)$	0.1185	$0.1165 - 0.1205$
f_s,strange fraction of $\bar{D}$	0.33	$0.25 - 0.40$
f_c,charm fraction of $\bar{U}$	0.15	$0.10 - 0.20$
m_c, GeV	1.4	$1.2 - 1.6$
m_b, GeV	4.5	$4.0 - 5.0$

Table 2: *Model uncertainties considered in the QCD analysis.*

5 Results

5.1 NC and CC Cross Sections $\mathrm{d}\sigma/\mathrm{dQ}^2$

The e^+p neutral current cross section $\mathrm{d}\sigma/\mathrm{dQ}^2$ from the 99-00 data is shown in fig.2(a). The data are compared to previous H1 e^+p measurements made at $\sqrt{s} \simeq 300$ GeV. The new cross sections are found to be higher than the measurement from $94 - 97$ as expected due to the increase in centre-of-mass energy. Both cross sections are well described by the Preliminary H1 2002 PDF Fit.

Fig.2 (b) shows the ratios of the measurements to the corresponding Standard Model expectation. The Standard Model uncertainty represents the effect of the assumptions and the experimental uncertainty of the QCD analysis and is detailed in section 4.2. The new data are observed to agree well with the previously published data. There is a tendency observed for the data to be larger than the expectation by a few percent which is consistent with the normalisation shift imposed by the QCD fit.

The Q^2 dependence of the charged current cross section from the 99-00 data is shown in fig.3(a) after correction for the kinematic cuts $0.03 < y < 0.85$ and $P_{T,h} > 12$ GeV using the Preliminary H1 2002 PDF Fit. The data are compared to the previous measurement taken at lower centre-of-mass energy. The ratio of data to expectation is shown in fig.3(b) together with the Standard Model uncertainty. The two data sets agree well with each other. At high Q^2 the data tend to be larger than the fit result which is essentially driven by the BCDMS data in this region.

Fig.4 shows the Q^2 dependence of the NC and CC cross sections representing the total e^+p and e^-p data sets taken in the first phase of HERA operation. At low Q^2 the NC cross section exceeds the CC cross section by more than two orders of magnitude. The sharp increase of the NC cross section with decreasing Q^2 is due to the dominating photon exchange cross section $\propto 1/Q^4$. In contrast, the CC cross section $\sim [M_W^2/(Q^2+M_W^2)]^2$ approaches a constant at low Q^2. The CC and NC cross sections are of comparable size at $Q^2 \sim 10^4$ GeV^2 where the photon and Z^0 exchange contributions to the NC process are also of similar size. These measurements thus demonstrate unification of the EW interaction in deep inelastic scattering. The difference of CC cross sections between e^+p and e^-p scattering is due to the different up and down quark densities and the less favourable helicity factor in e^+p interactions.

5.2 NC and CC Double Differential Cross Sections

The double differential NC reduced cross section, $\tilde{\sigma}_{NC}$ (defined in eq. 9), is shown in fig. 5 for the $99-00$ e^+p data for both the nominal and high-y analyses (see section 3.3). In addition the high-y analysis results of the $98-99$ e^-p data are presented. The data agree well with the predictions of the Preliminary H1 2002 PDF Fit which is also shown[2]. The rise of the Standard Model cross section towards low x departs from a monotonic behaviour at the lowest x due to the contribution of the longitudinal structure function that enters approximately $\propto y^2$.

In fig 6 the new e^+p NC cross section data at $\sqrt{s} \simeq 320$ GeV are compared with the data obtained previously [1] at $\sqrt{s} \simeq 300$ GeV. The two data sets are found to be in agreement with each other and with the Preliminary H1 2002 PDF Fit. Fig.6 also shows the data from recent H1 measurement at lower Q^2 [28] and the fixed-target data from BCDMS [3]. At the highest Q^2 a decrease of the cross section is expected due to the negative γZ interference in e^+p scattering which needs still higher luminosity to be studied in detail.

In fig. 7 the reduced CC cross section, $\tilde{\sigma}_{CC}$ (defined in eq. 9), is shown for the new data and the data taken in $94-97$. These data are found to be consistent. The combined result is thus shown in fig. 8 and is well described by the Preliminary H1 2002 PDF Fit.

5.3 Extraction of the Proton Structure Functions F_2 and F_L

The measured NC double differential cross section is dominated by the structure function F_2 in most of the kinematic range. In order to extract F_2 the reduced cross section must be corrected for the contribution from the other structure functions and for Z^0 exchange according to the equation

$$\tilde{\sigma}_{NC} = F_2(1+\Delta_{F_2}+\Delta_{F_3}+\Delta_{F_L})(1+\Delta_{NC}^{weak}) = F_2(1+\Delta_{all}) \quad . \tag{18}$$

Here the correction terms Δ_{F_2} and Δ_{F_3} account for the relative contribution of pure Z^0 exchange and γZ^0 interference to $\tilde{F}_2$ and $x\tilde{F}_3$, whilst Δ_{F_L} originates from the longitudinal structure function $\tilde{F}_L$. Δ_{all} represents the combination of these corrections with the weak radiative corrections. At high y and low $Q^2(\lesssim 1000\ \mathrm{GeV}^2)$ Δ_{F_L} is sizeable thus allowing the cross section measurement to be used to determine F_L. The extraction of F_2 in this Q^2 region is restricted to

[2]Note, the normalisation as determined by the QCD fit is not applied to the data shown in the figure.

the kinematic range $y < 0.6$. It is extended to higher y at larger Q^2 in order to study the scaling violations.

Fig.9 shows the extracted F_2 data using the combined $94-97$ and $99-00$ high Q^2 e^+p data sets. In addition the figure also shows the recent H1 F_2 measurements at lower Q^2. The H1 data cover a range of five orders of magnitude in x and Q^2. The Preliminary H1 2002 PDF fit is able to provide a good description of the data over the full region, and in particular of the scaling violations observed in the measurements.

As stated above the cross sections at high $y > 0.63$ and $Q^2 \lesssim 1000$ GeV^2 are used here to determine F_L. In order to optimise the sensitivity to F_L, the measured cross sections in two neighbouring Q^2 bins are combined. Statistical errors are added in quadrature and systematic uncertainties are assumed to be fully correlated between the two bins. F_L is then determined from the measured reduced cross sections after combination using the formula:

$$\tilde{F}_L = \frac{Y_+}{y^2}\left[\tilde{F}_2 - \frac{Y_-}{Y_+}x\tilde{F}_3 - \tilde{\sigma}_{NC}\right] \ . \tag{19}$$

The extraction of F_L using eq. 19 relies upon the extrapolation of F_2 into the high y region. In the kinematic range considered the EW contributions to eq. 19 are small and are corrected for. This equation reduces to

$$F_L = \frac{Y_+}{y^2}\left[F_2 - \frac{\tilde{\sigma}_{NC}}{1+\Delta_{NC}^{weak}}\right] \ , \tag{20}$$

where F_2 is determined from a dedicated QCD fit to H1 data only, restricted to $y < 0.35$ [39]. This fit follows exactly the same procedure as described in section 4. It results in a χ^2/ndf$=424/(455-15) = 0.96$ and agrees with the H1 only fit over the full y range.

In the extraction of the longitudinal structure function the experimental cross sections are renormalised using the results of the fit. In addition small shifts of the data arising from the optimised correlated systematic uncertainties are applied. This is necessary in order to have a consistent description of the data at low $y < 0.35$ and at high y. The uncertainties on F_L due to the correlation of systematic error sources common to the region $y < 0.35$ and high y are taken into account. The additional systematic uncertainty due to the background charge asymmetry is added in quadrature.

In fig.10 the determinations of F_L at high Q^2 are shown at fixed $y = 0.75$ for both the e^+p and the e^-p data sets. The results from both data sets are mutually consistent and are in agreement with the Preliminary H1 2002 PDF Fit. The extreme values allowed for F_L ($F_L = 0$ and $F_L = \tilde{F}_2$) are clearly excluded by the data.

5.4 The Quark Distributions xu and xd at Large x

The flavour composition of the proton at high x may be disentangled by exploiting the NC and CC cross section measurements. The e^+p CC cross section at large x is dominated by the d quark contribution as may be inferred from fig. 8. Similarly the u density dominates the e^-p CC cross section. In addition the e^+p and e^-p NC cross sections are dominated by the u density at high enough x for the sea to be neglected. Requiring the u or d contribution to provide a minimum 70% of the cross section, as inferred from the Preliminary H1 2002 PDF Fit, allows the up and down quarks to be determined locally. The extraction relies on weighting the differential cross section measurement with the expected local flavour contribution and is illustrated in fig. 11. The method of extraction relies directly on the *local* cross section measurements and is complementary to performing a QCD fit since the extraction is insensitive to QCD assumptions.

The data are compared to the results of the Preliminary H1 2002 PDF Fit and to other global parameterisations from the MRST [37] and CTEQ [38] collaborations. This procedure is an indirect determination of the u and d distributions in the valence quark region. Note, however, that the separation between quarks and anti-quarks, and thus the extraction of the valence quark distributions, is entirely dependent to the helicity structure of the CC cross sections and the Z^0 exchange parts of the NC cross section. A measurement of the valence quark densities from H1 data alone must be deferred to the high luminosity phase of HERA.

6 Summary

New data are presented on inclusive deep inelastic neutral and charged current scattering cross sections at high momentum transfers $Q^2 > 100\,\mathrm{GeV}^2$ from recent $(1999-2000)$ positron-proton runs at HERA with a luminosity of 65.2 pb^{-1}. These data taken together with previous analyses of the $1994 - 1997$ e^+p data (35.6 pb^{-1}) and $1998 - 1999$ e^-p runs (16.4 pb^{-1}) represent the now complete analysis of the high Q^2 data obtained during the first phase of HERA operation over nearly a decade of data taking.

The accuracy of the NC measurements presented here has reached the level of a few $\%$ in the mid Q^2 range of $Q^2 < 3000\,\mathrm{GeV}^2$, a precision which is largely due to a better understanding of the LAr calorimeter performance and calibration of the electromagnetic and the hadronic energy scales. Both the CC and the very high Q^2 ($Q^2 > M_Z^2$) NC data are still limited by their statistical accuracy to about $10-20\%$ uncertainties which are expected to be diminished in the future high luminosity phase of HERA.

For both positron and electron scattering data the region of very large inelasticity is explored which allows a determination of the longitudinal structure function $F_L(x, Q^2)$ in the large momentum transfer range, $100 < Q^2 < 700$ GeV^2.

The NC and CC cross sections at high Q^2 measure linear combinations of the sums of up and down quark and antiquark momentum densities, $U, D, \bar{U}$, and $\bar{D}$. Introducing these four distributions into the minimisation procedure, a novel NLO QCD analysis is performed aiming at a determination of the partonic nucleon structure from inclusive DIS scattering data alone. In this Preliminary H1 2002 PDF fit the low Q^2 region is constrained by recent H1 ep scattering data at low x and by muon-nucleon data of the BCDMS collaboration at high x.

The QCD analysis leads to a good description of all the NC and CC cross section data and of the derived structure functions over the large range of nearly five orders of magnitude in x and Q^2. The analysis presented here leads to the first simultaneous unfolding of four quark distributions and the gluon distribution with consistent results from the analysis of H1 data alone with the Preliminary H1 2002 PDF fit.

Acknowledgments

We are grateful to the HERA machine group whose outstanding efforts have made and continue to make this experiment possible. We thank the engineers and technicians for their work in constructing and now maintaining the H1 detector, our funding agencies for financial support, the DESY technical staff for continual assistance, and the DESY directorate for the hospitality which they extend to the non DESY members of the collaboration.

References

[1] C. Adloff *et al.* [H1 Collaboration], Eur. Phys. J. C **13** (2000) 609 [hep-ex/9908059].

[2] J. Breitweg *et al.* [ZEUS Collaboration], Eur. Phys. J. C **11** (1999) 427 [hep-ex/9905032].
J. Breitweg *et al.* [ZEUS Collaboration], Eur. Phys. J. C **12** (2000) 411 [hep-ex/9907010].

[3] A. C. Benvenuti *et al.* [BCDMS Collaboration], Phys. Lett. B **223** (1989) 485.

[4] C. Adloff *et al.* [H1 Collaboration], Eur. Phys. J. C **19** (2001) 269 [hep-ex/0012052].

[5] S. Bentvelsen et. al., Proceedings of the Workshop "Physics at HERA", vol. 1, eds. W. Buchmüller, G. Ingelman, DESY (1992) 23; C. Hoeger, ibid., 43.

[6] H. Spiesberger et al., Proceedings of the Workshop "Physics at HERA", vol. 2, eds. W. Buchmüller, G. Ingelman, DESY (1992) 798.

[7] M. Klein and T. Riemann, Z. Phys. C **24** (1984) 151.

[8] D. E. Groom *et al.* [Particle Data Group Collaboration], Eur. Phys. J. C **15** (2000) 1.

[9] I. Abt *et al.* [H1 Collaboration], Nucl. Instrum. Meth. A **386** (1997) 310. I. Abt *et al.* [H1 Collaboration], Nucl. Instrum. Meth. A **386** (1997) 348.

[10] R. D. Appuhn *et al.* [H1 SPACAL Group Collaboration], Nucl. Instrum. Meth. A **386** (1997) 397.

[11] G.A. Schuler and H. Spiesberger, Proceedings of the Workshop "Physics at HERA", vol. 3, eds. W. Buchmüller, G. Ingelman, DESY (1992) 1419.

[12] A. Kwiatkowski, H. Spiesberger and H. J. Mohring, Comput. Phys. Commun. **69** (1992) 155.

[13] G. Ingelman, Proceedings of the Workshop "Physics at HERA", vol. 3 eds. W. Buchmüller, G. Ingelman, DESY (1992) 1366.

[14] L. Lönnblad, Comput. Phys. Commun. **71** (1992) 15.

[15] T. Sjöstrand and M. Bengtsson, Comput. Phys. Commun. **43** (1987) 367.

[16] R. Brun et al., GEANT3 User's Guide, CERN-DD/EE-84-1 (1987).

[17] T. Sjöstrand, Comput. Phys. Commun. **82** (1994) 74.

[18] M. Glück, E. Reya and A. Vogt, Phys. Rev. D **46** (1992) 1973.

[19] U. Bassler and G. Bernardi, Z. Phys. C **76** (1997) 223 [hep-ex/9707024].

[20] B. Reisert, Ph.D. Thesis, Max-Planck-Institut für Physik,Munich, MPI-PhE/2000-26. Also available at http://www-h1.desy.de/publications/theses_list.html

[21] A. Dubak, Ph.D. Thesis, Max-Planck-Institut für Physik, Munich, *in preparation.*

[22] U. Bassler and G. Bernardi, Nucl. Instrum. Meth. A **361** (1995) 197 [hep-ex/9412004].
U. Bassler and G. Bernardi, Nucl. Instrum. Meth. A **426** (1999) 583 [hep-ex/9801017].

[23] J. Rauschenberger, Ph.D. Thesis, Hamburg University, 2002. Also available at http://www-h1.desy.de/publications/theses_list.html

[24] Z. Zhang, Habilitation Thesis, LAL, 2000, LAL 00-57.

[25] A. Blondel and F. Jacquet, Proceedings of the Study of an ep Facility for Europe, ed. U. Amaldi, DESY 79/48 (1979) 391.

[26] A. Arbuzov, D. Y. Bardin, J. Bluemlein, L. Kalinovskaya and T. Riemann, scattering," Comput. Phys. Commun. **94** (1996) 128 [hep-ph/9511434].

[27] B. Heinemann, Ph.D. Thesis, Hamburg University, 1999, DESY-THESIS-1999-046. Also available at http://www-h1.desy.de/publications/theses_list.html

[28] C. Adloff *et al.* [H1 Collaboration], Eur. Phys. J. C **21** (2001) 33 [hep-ex/0012053].

[29] W. Melnitchouk and A. W. Thomas, Phys. Rev. C **52** (1995) 3373 [hep-ph/9508311].

[30] C. Adloff *et al.* [H1 Collaboration], Phys. Lett. B **528** (2002) 199[hep-ex/0108039].

[31] J. Breitweg *et al.* [ZEUS Collaboration], Eur. Phys. J. C **12** (2000) 35 [hep-ex/9908012].

[32] M. Goncharov *et al.* [NuTeV Collaboration], Phys. Rev. D **64** (2001) 112006 [hep-ex/0102049].

[33] Y. L. Dokshitzer, Sov. Phys. JETP **46** (1977) 641 [Zh. Eksp. Teor. Fiz. **73** (1977) 1216];
V. N. Gribov and L. N. Lipatov, Yad. Fiz. **15** (1972) 1218 [Sov. J. Nucl. Phys. **15** (1972) 675];
V. N. Gribov and L. N. Lipatov, Yad. Fiz. **15** (1972) 781 [Sov. J. Nucl. Phys. **15** (1972) 438];
G. Altarelli and G. Parisi, Nucl. Phys. B **126** (1977) 298.

[34] W. Furmanski and R. Petronzio, Phys. Lett. B **97** (1980) 437.

[35] C. Pascaud and F. Zomer, LAL preprint, LAL/95-05 (1995)

[36] M. Botje, QCDNUM15 program, *write-up in preparation*; J. Blümlein et al., Proceedings of the Workshop "Future Physics at HERA", vol. 1, eds. G. Ingelman, A. De Roeck, R. Klanner, DESY (1996) 23.

[37] A. D. Martin, R. G. Roberts, W. J. Stirling and R. S. Thorne, Eur. Phys. J. C **23** (2002) 73 [hep-ph/0110215].

[38] J. Pumplin, D. R. Stump, J. Huston, H. L. Lai, P. Nadolsky and W. K. Tung, JHEP **0207** (2002) 012 [hep-ph/0201195].

[39] C. Adloff *et al.* [H1 Collaboration], Phys. Lett. B **393** (1997) 452 [hep-ex/9611017].

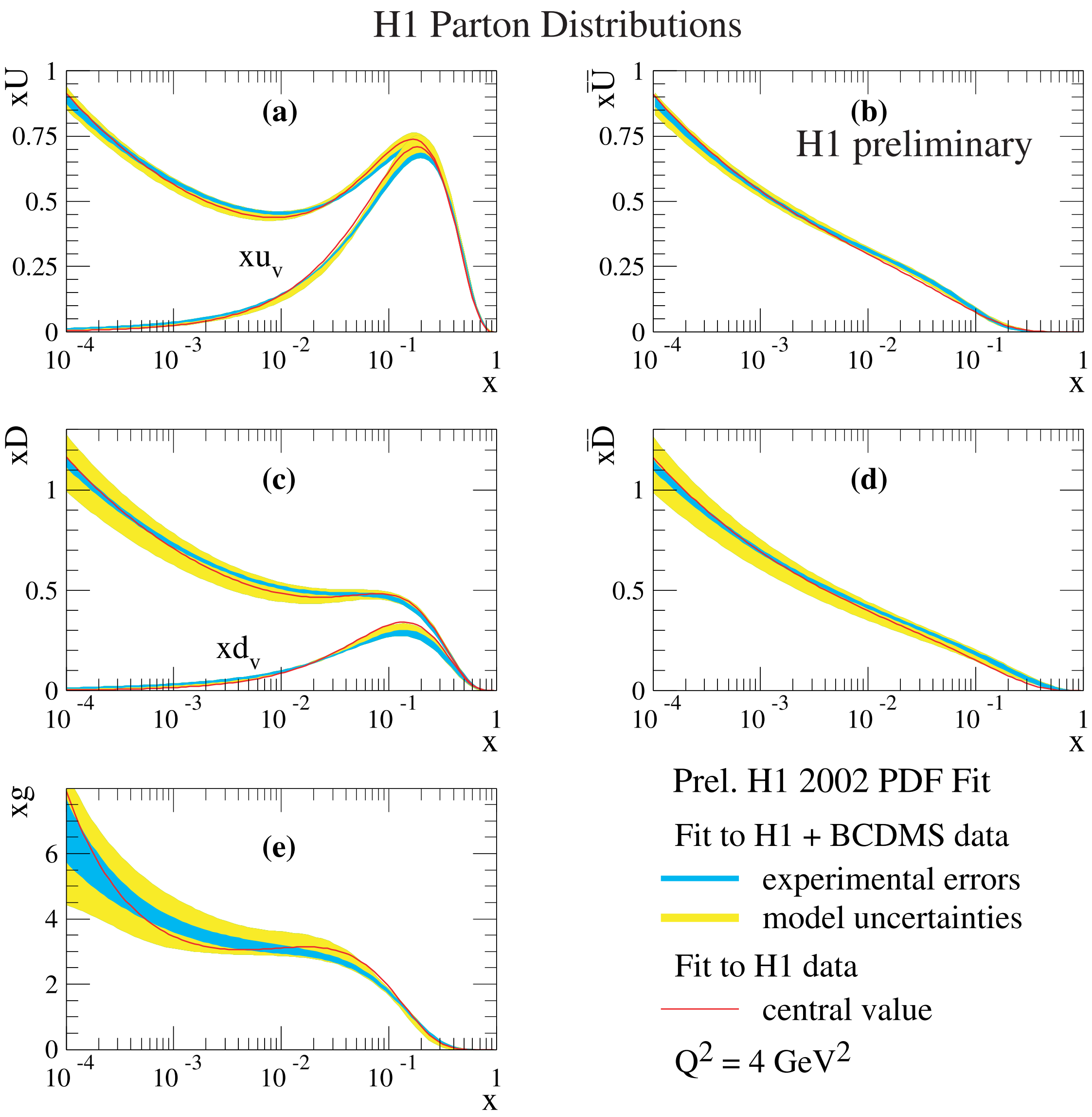

Figure 1: Parton distributions (a) xU, (b) $x\bar{U}$,(c) xD, (d) $x\bar{D}$, and (e) xg as determined from the Preliminary H1 2002 PDF Fit to H1 and BCDMS data. The distributions are shown at $Q^2 = 4$ GeV^2 with experimental and model uncertainties. The valence quark densities xu_v (a) and xd_v (c) are also shown. determined with H1 and BCDMS. For comparison, the central values from the fits to H1 data alone are also shown.

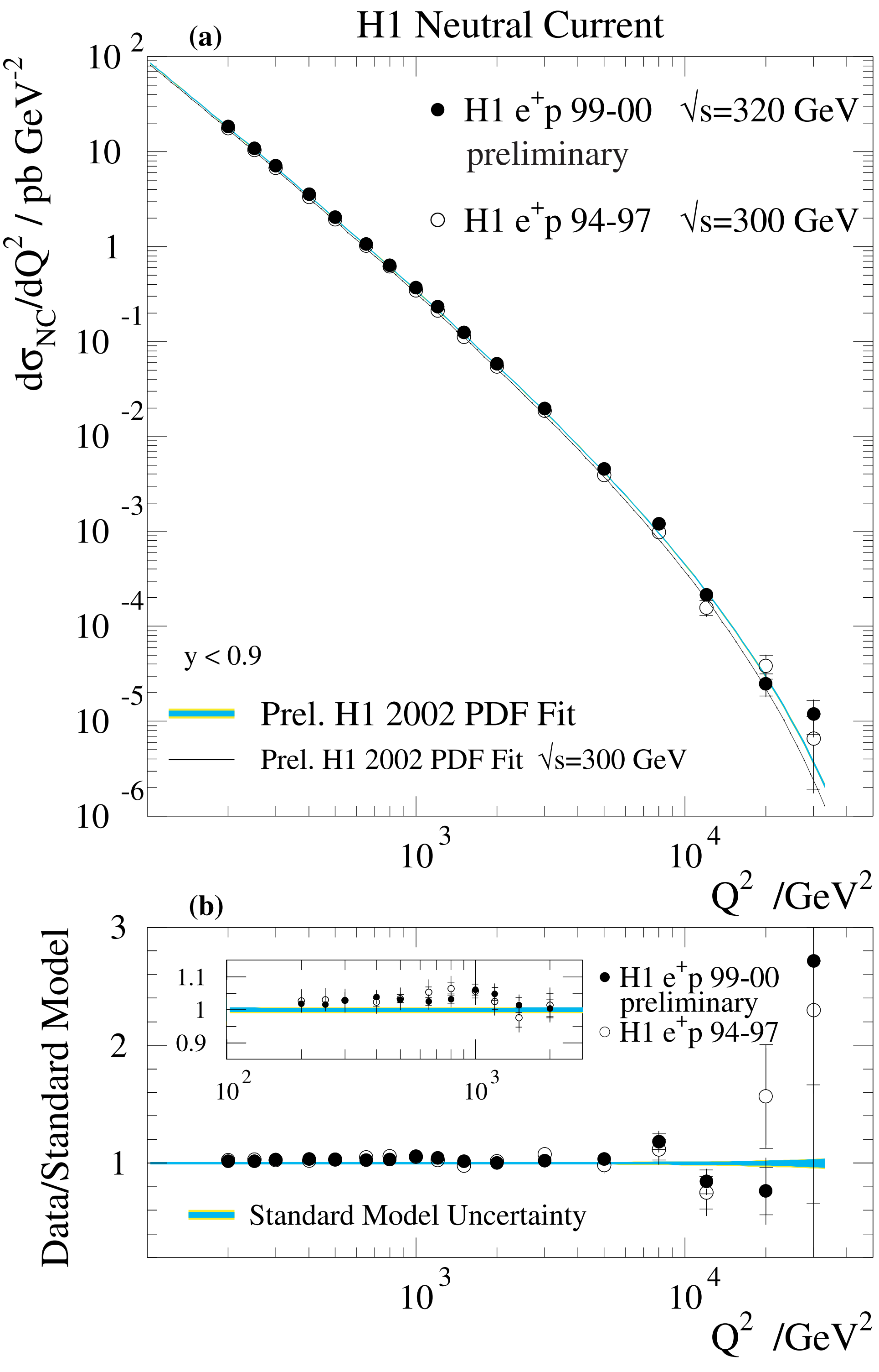

Figure 2: *The Q^2 dependence of NC cross sections $d\sigma/dQ^2$ is shown for the new preliminary e^+p (solid points) and published $94-97$ e^+p (open points) measurements. The data are compared to the Standard Model expectation determined from the Preliminary H1 2002 PDF Fit. The full (dashed) line corresponds to a center-of-mass energy of $\sqrt{s} \simeq 300$ GeV ($\sqrt{s} \simeq 320$ GeV). The ratio of the $94-97$ and $99-00$ data to their respective Standard Model expectations is shown in (b). The Standard Model uncertainty is shown as the shaded band. The 1.5% luminosity uncertainty is not included in the error bars.*

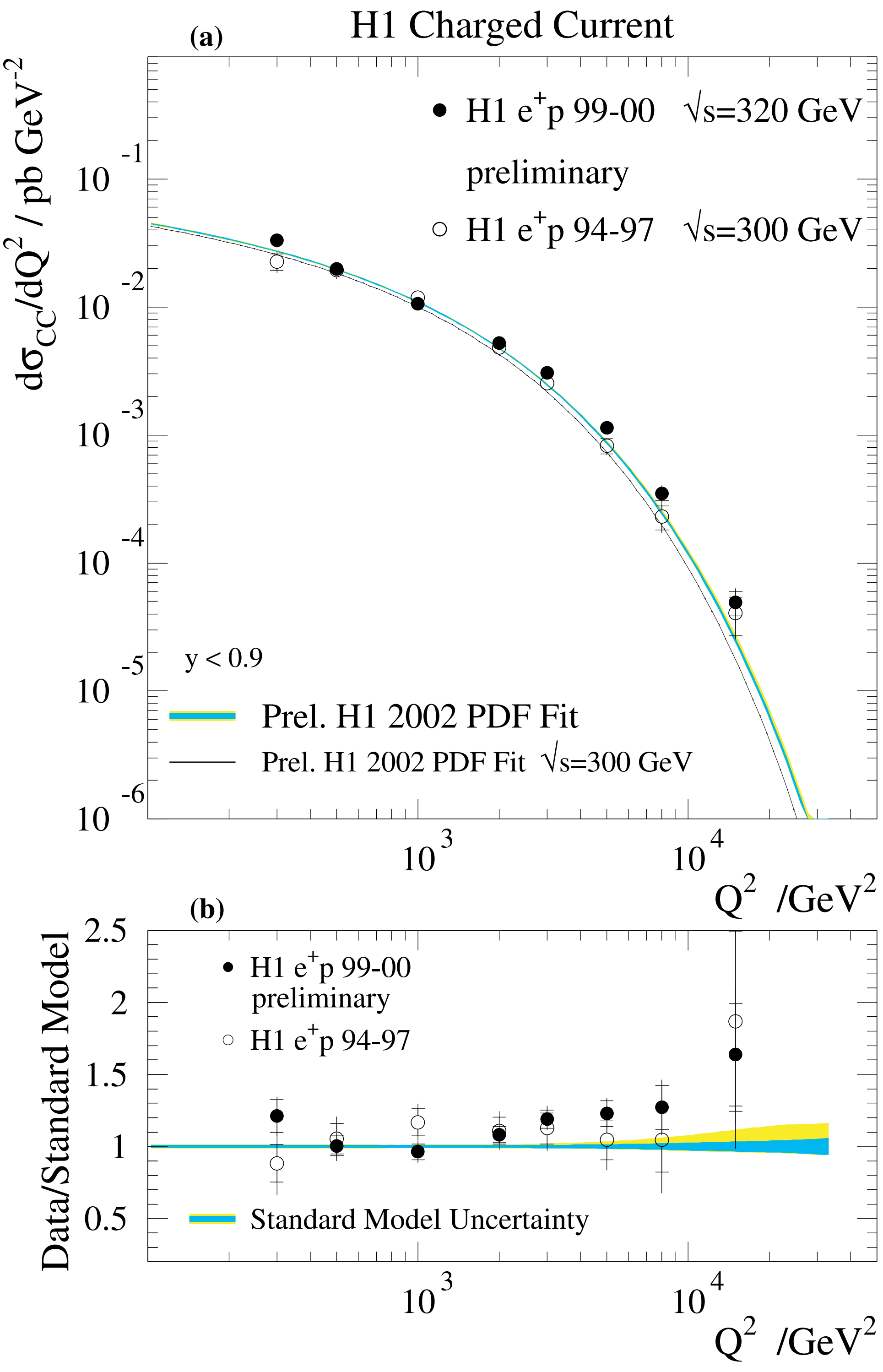

Figure 3: *The Q^2 dependence of CC cross section $d\sigma/dQ^2$ is shown for the new preliminary e^+p (solid points) and published $94-97$ e^+p (open points) measurements. The data are compared to the Standard Model expectation determined from the Preliminary H1 2002 PDF Fit. The full (dashed) line corresponds to a center-of-mass energy of $\sqrt{s} \simeq 300$ GeV ($\sqrt{s} \simeq 320$ GeV). The ratio of the $94-97$ and $99-00$ data to their respective Standard Model expectations is shown in (b). The Standard Model uncertainty is shown as the shaded band. The 1.5% luminosity uncertainty is not included in the error bars.*

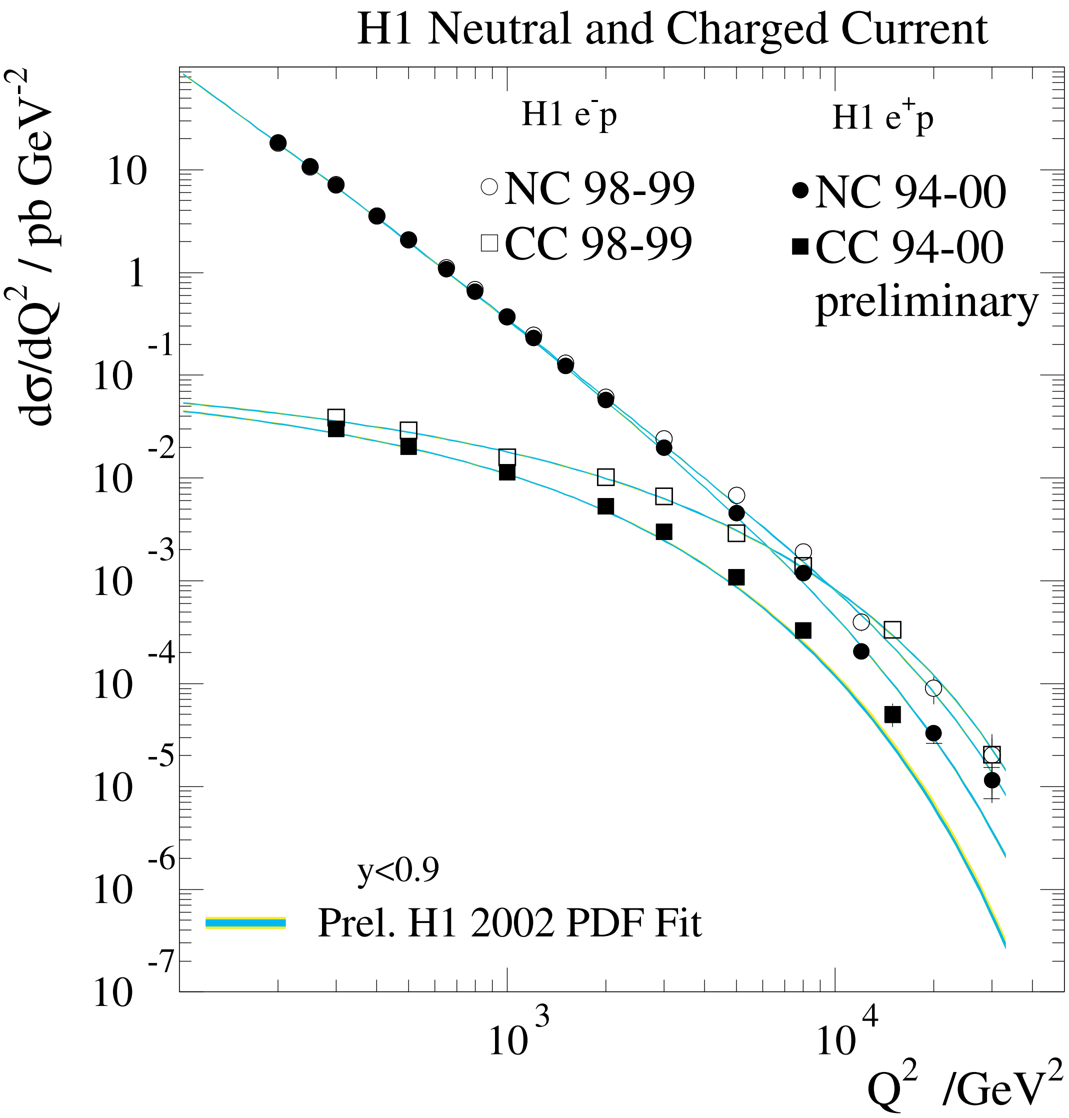

Figure 4: *The Q^2 dependences of the NC (circles) and CC (squares) cross sections $d\sigma/dQ^2$ are shown for the combined $94-00$ e^+p (solid points) and e^-p (open points) measurements. The data are compared to the Standard Model expectations determined from the Preliminary H1 2002 PDF Fit. The 1.5% luminosity uncertainty is not included in the error bars.*

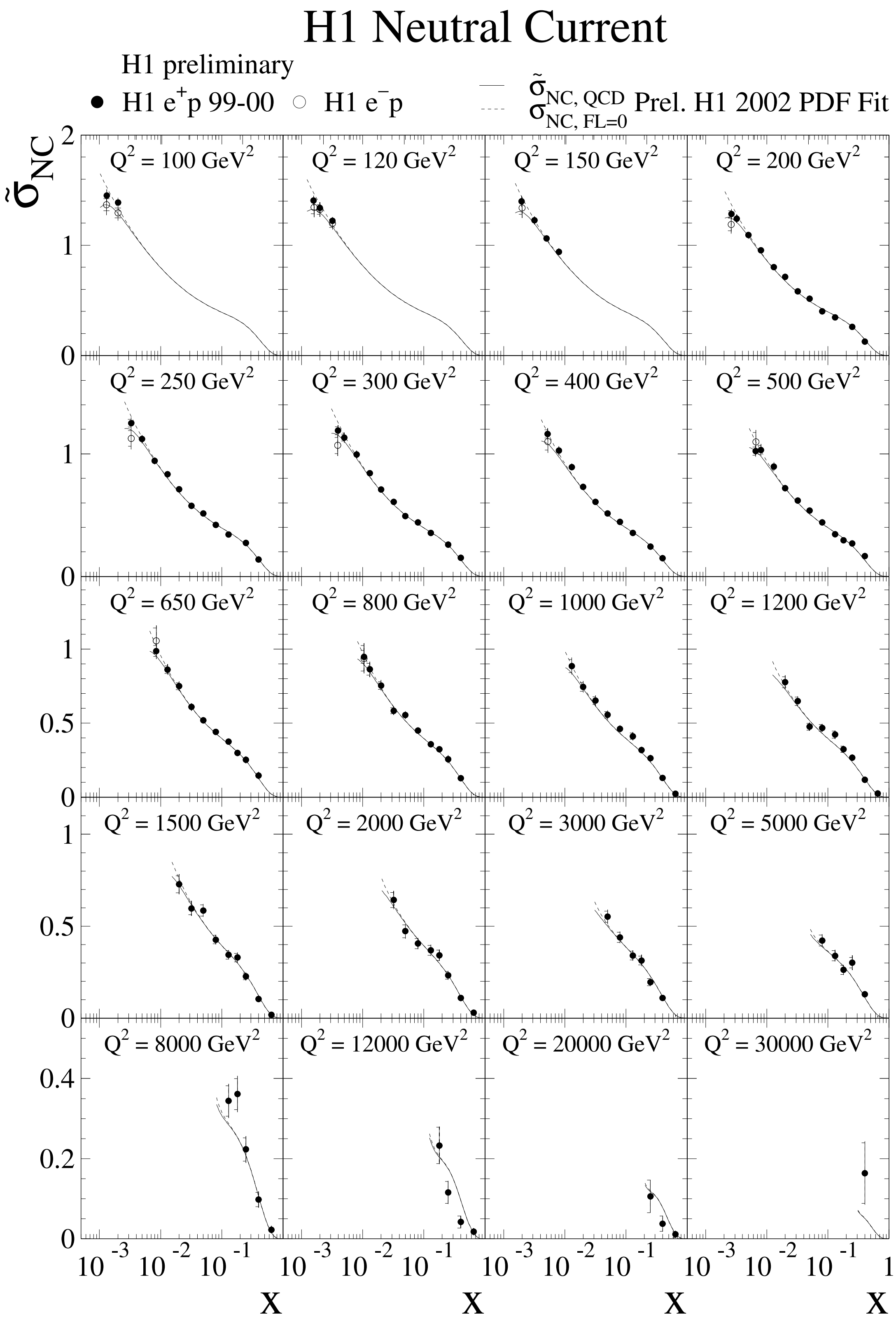

Figure 5: *The NC reduced cross section $\tilde{\sigma}_{NC}$ is compared to the Preliminary H1 2002 PDF Fit. The* $99-00$ e^+p *data and the* high-y analysis e^-p *data of* $98-99$ *data are shown. The inner error bars represent the statistical error, and the outer error bars show the total error. The 1.5% luminosity uncertainty is not included in the error bars.*

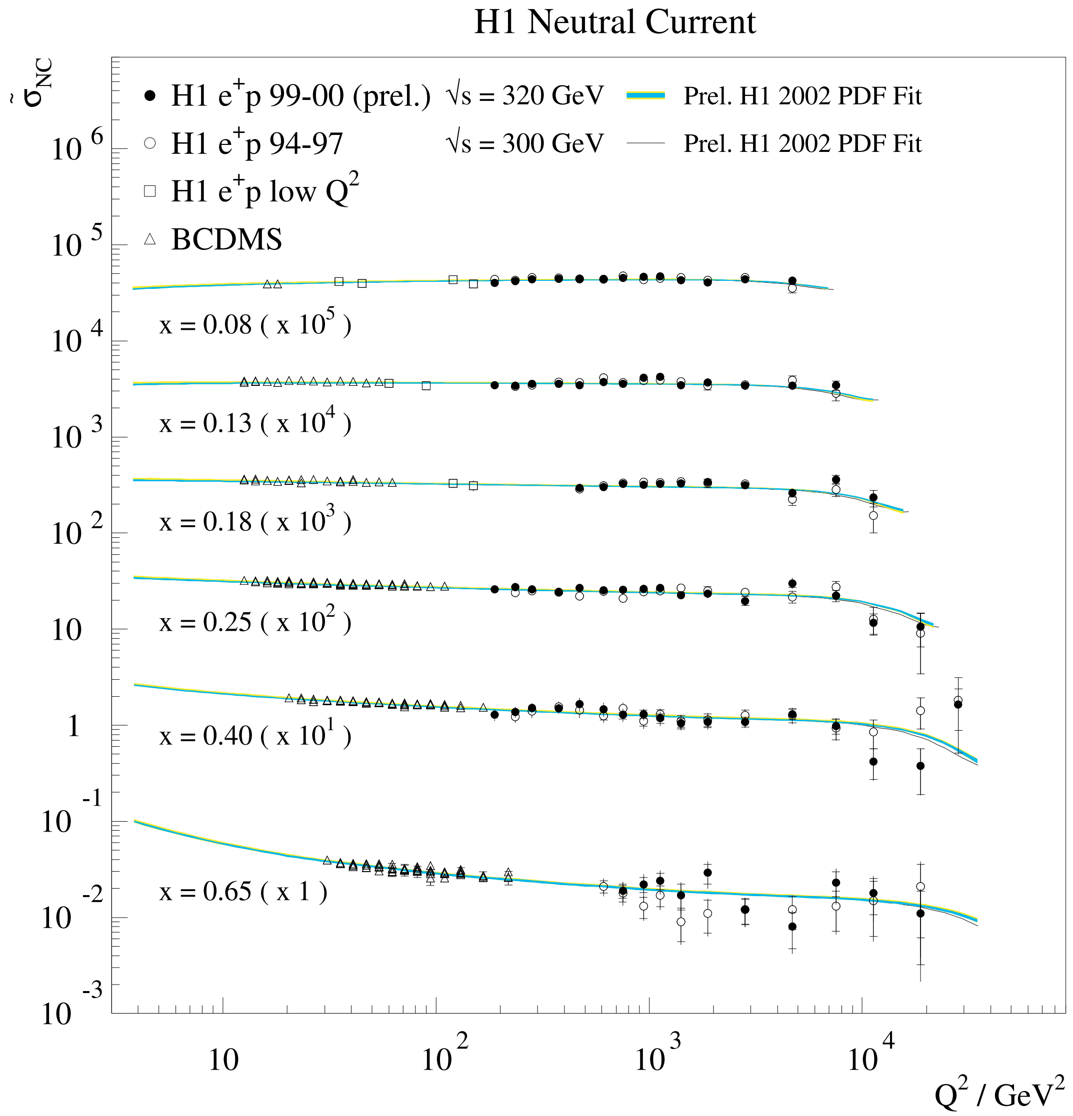

Figure 6: *The NC reduced cross sections $\tilde{\sigma}_{NC}$ from the $94-97$ and $99-00$ e^+p data are shown at high x compared to the Preliminary H1 2002 PDF Fit. Also shown are data from H1 measured at lower Q^2, as well as from the fixed-target experiment BCDMS. The dashed (solid) curve represents the Standard Model expectation based on the Preliminary H1 2002 PDF Fit for $\sqrt{s} \simeq 320$ GeV ($\sqrt{s} \simeq 300$ GeV). The inner error bars represent the statistical error, and the outer error bars show the total error. The 1.5% luminosity uncertainty is not included in the error bars.*

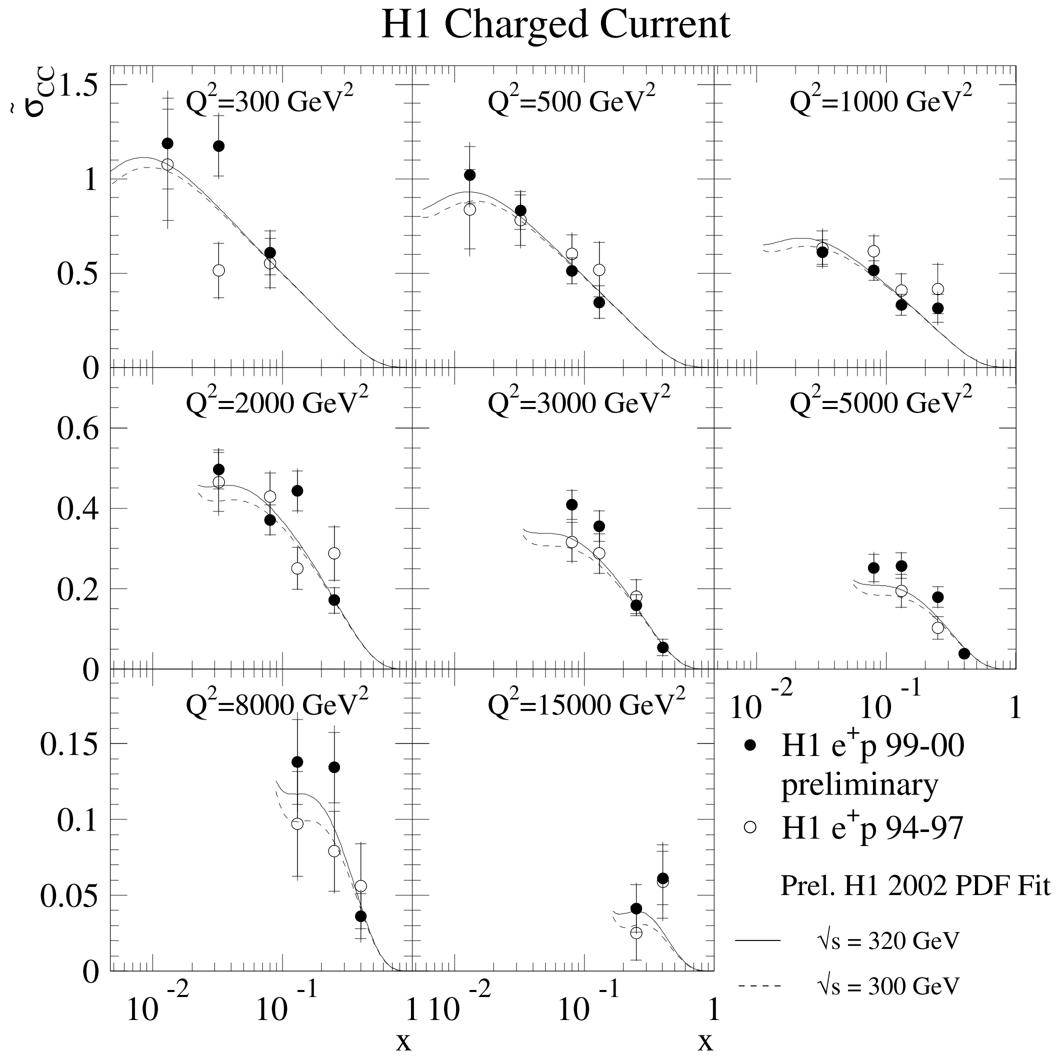

Figure 7: *The CC reduced cross section $\tilde{\sigma}_{CC}(x, Q^2)$ is shown for e^+p scattering for the new data from $99-00$ at $\sqrt{s} \simeq 320$ GeV (solid circles) and the data from $94-97$ at $\sqrt{s} \simeq 300$ GeV (open circles). The data are compared to the Preliminary H1 2002 PDF Fit with the full and dashed curves showing respectively predictions for $\sqrt{s} \simeq 320$ GeV and $\sqrt{s} \simeq 300$ GeV. The inner error bars represent the statistical error, and the outer error bars show the total error. The 1.5% luminosity uncertainty is not included in the error bars.*

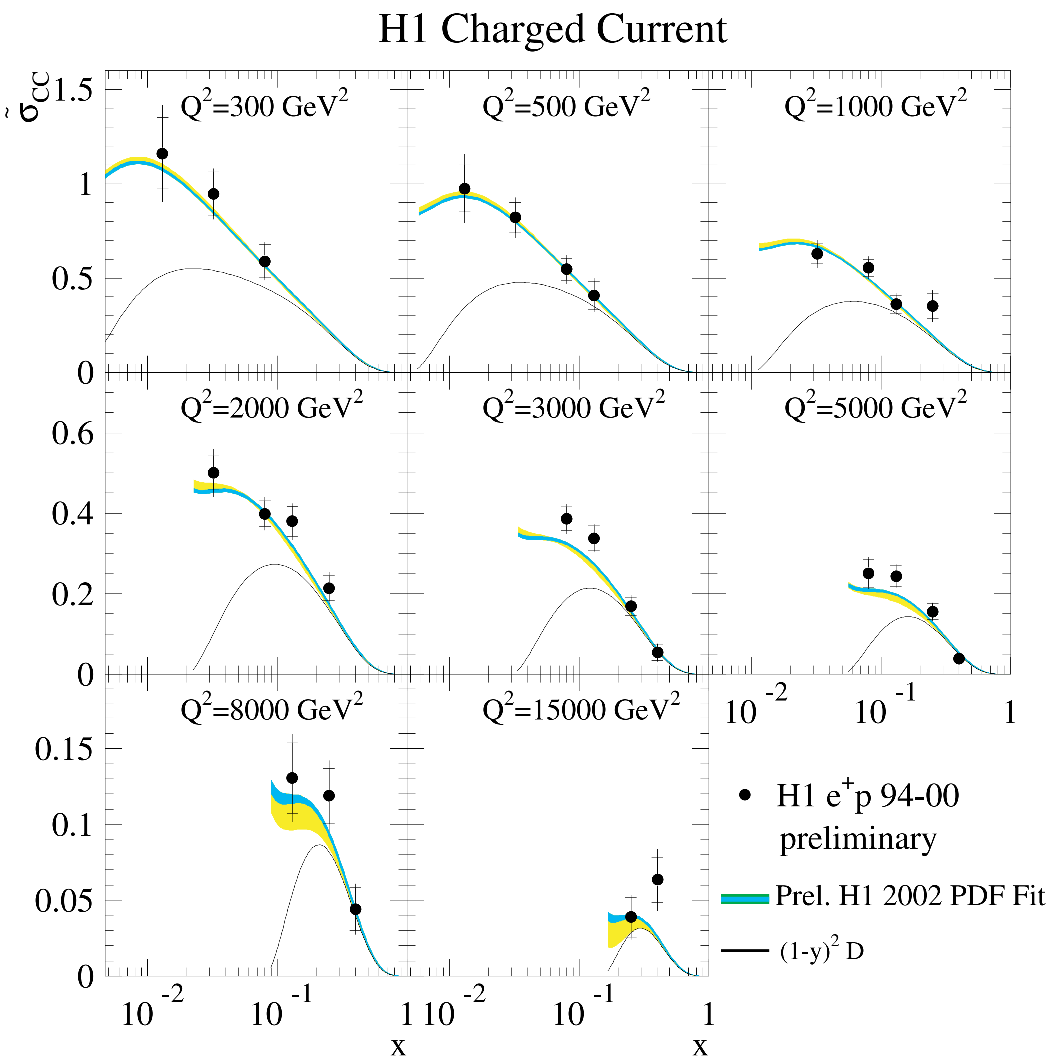

Figure 8: *The CC reduced cross section* $\tilde{\sigma}_{CC}(x, Q^2)$ *for* e^+p *scattering is shown for the combined data from* $94 - 00$ *at* $\sqrt{s} \simeq 320$ *GeV. The full line shows the Preliminary H1 2002 PDF Fit and the dashed curve indicates the* d *contribution in that model. The inner error bars represent the statistical error, and the outer error bars show the total error. The 1.5% luminosity uncertainty is not included in the error bars.*

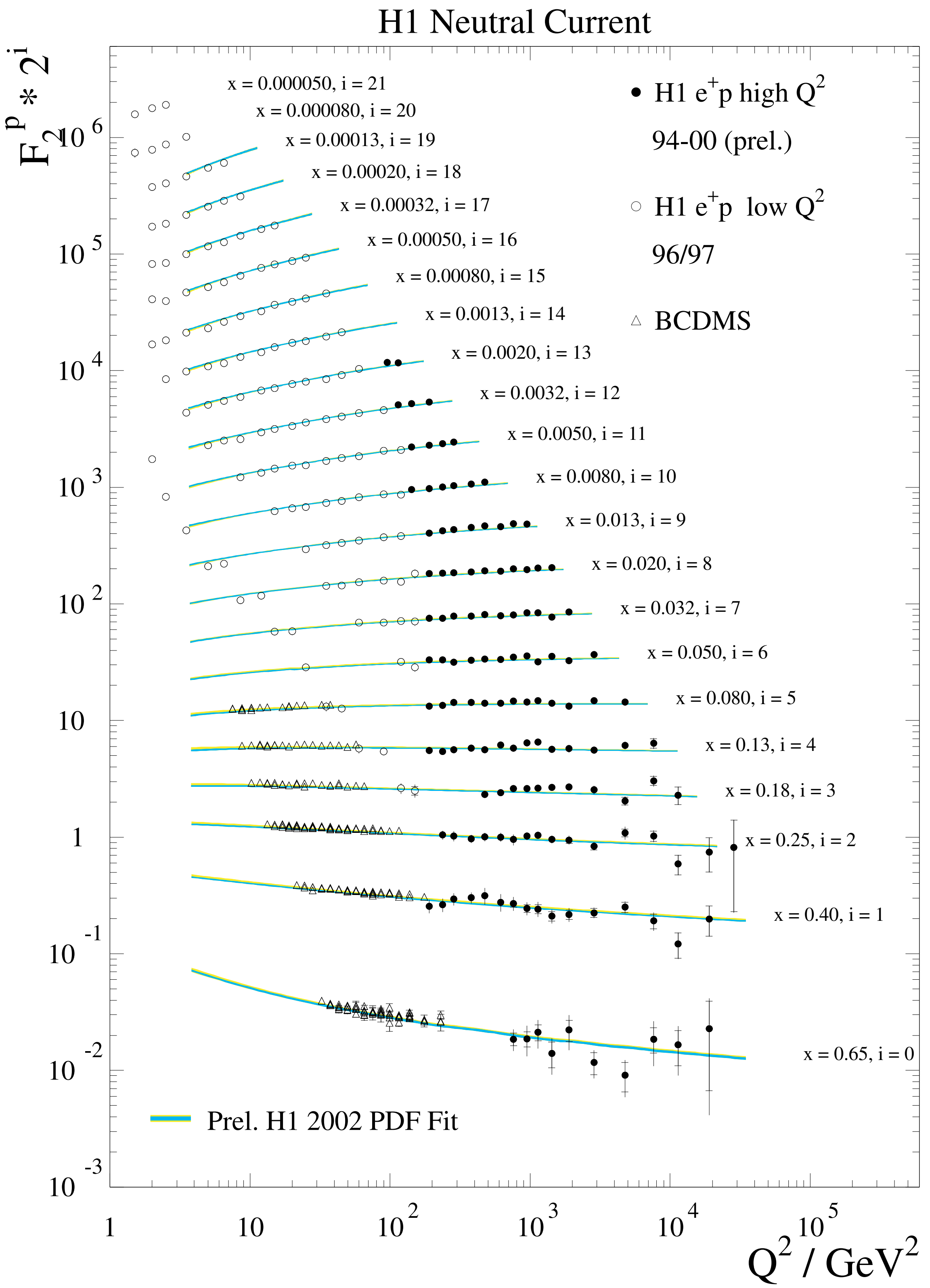

Figure 9: *The proton structure function F_2 from H1 data compared to the Preliminary H1 2002 PDF Fit. Also shown are the F_2 μp scattering measurements from BCDMS.*

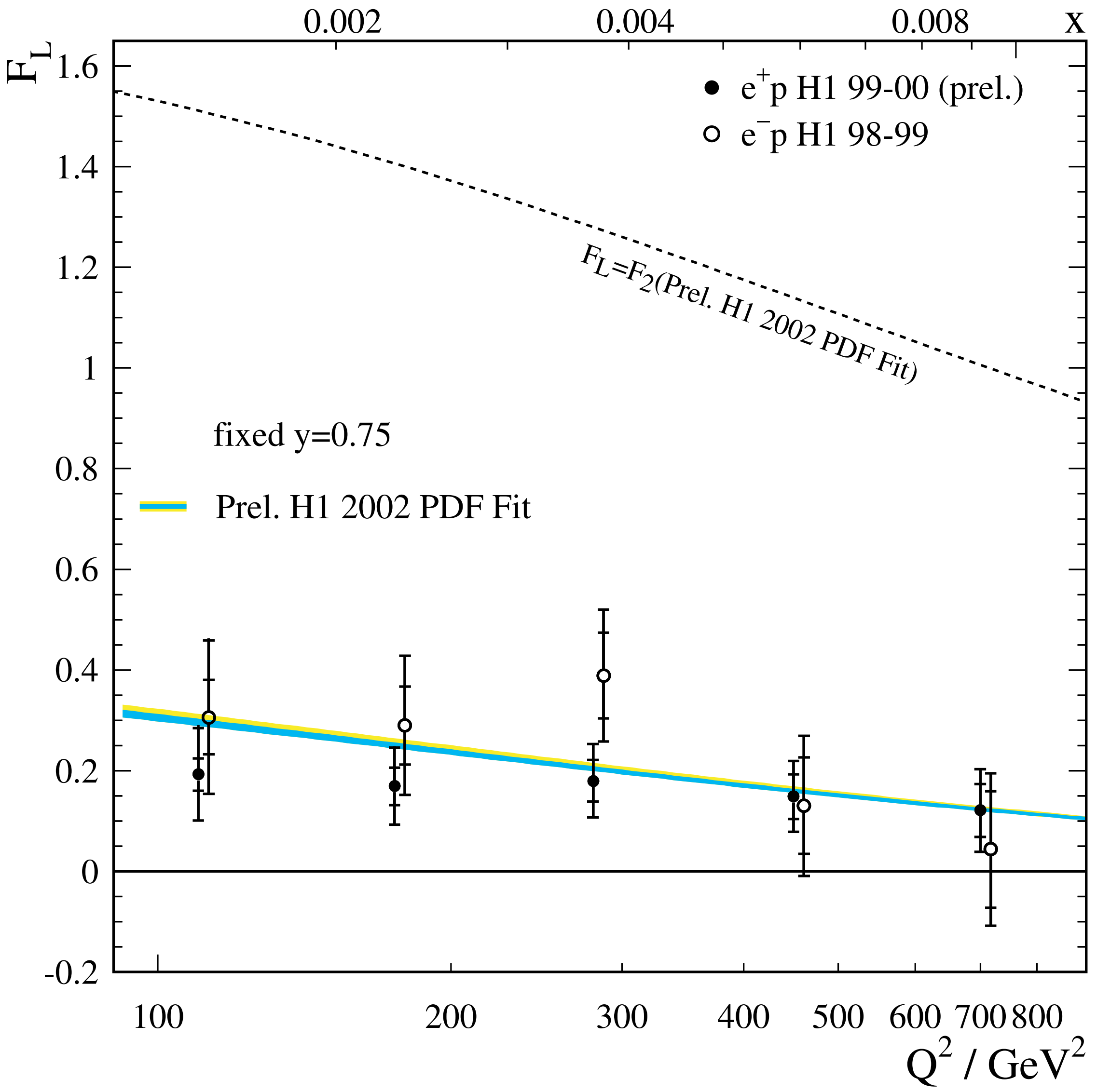

Figure 10: *Determination of F_L shown for e^-p and e^+p data at fixed $y = 0.75$ as a function of Q^2 (lower scale), or equivalently x (upper scale). The inner error bar represents the statistical error, the intermediate error bar shows the systematic uncertainty contribution, and the outer error bar includes the uncertainty arising from the extrapolation of F_2. The lower shaded band shows the expectation of F_L, and its uncertainty, from the Preliminary H1 2002 PDF fit. The upper shaded band shows the F_2 extrapolation at $y = 0.75$. This is theoretically the maximum allowed value for F_L.*

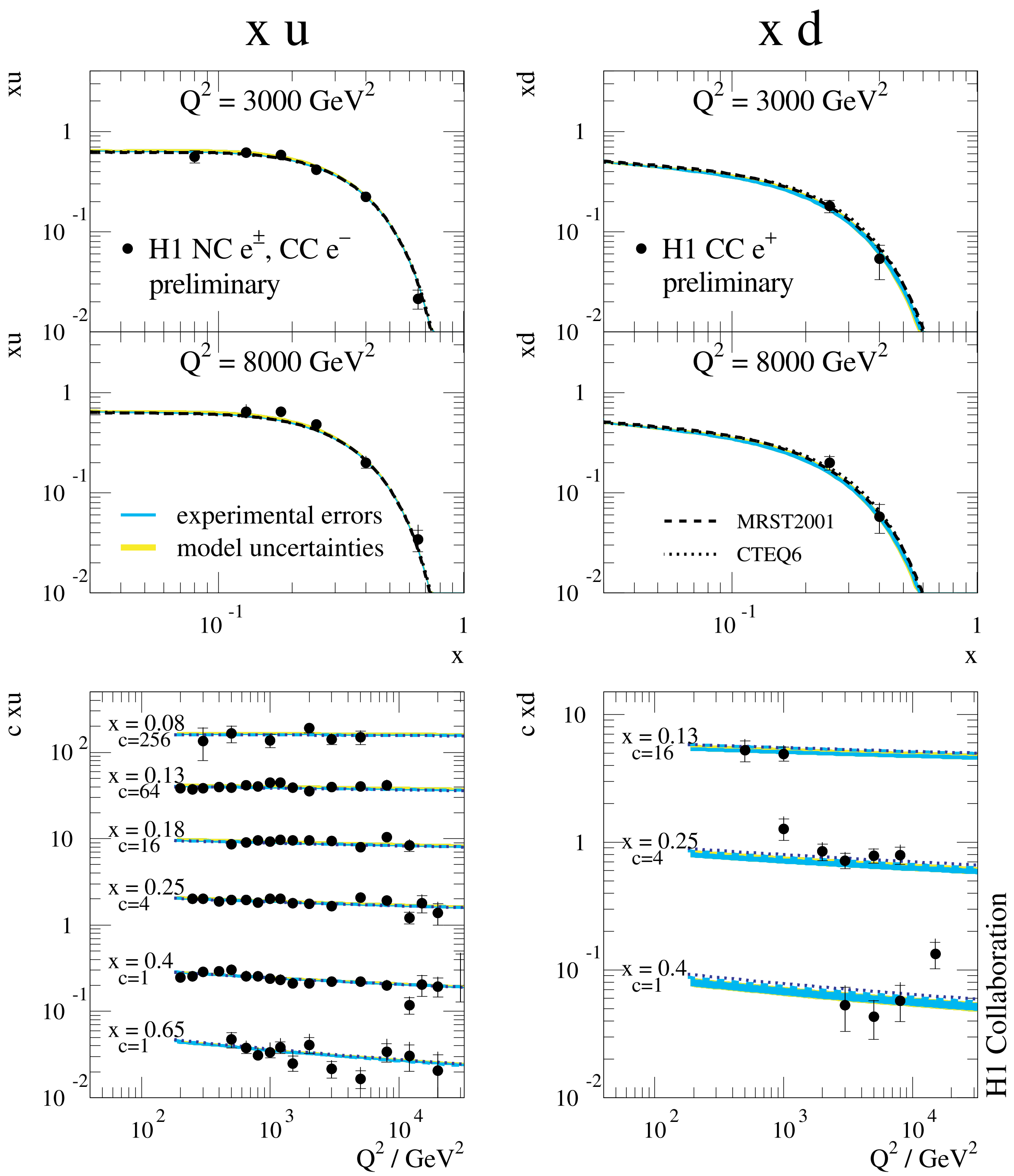

Figure 11: *The quark distributions xu and xd determined both with the Preliminary H1 2002 PDF fit (shaded error bands) using all cross section measurements from H1 only and with the local extraction method (data points with the inner and full error bars showing respectively the statistical and total errors) in comparison with other parameterisations which included data from a variety of other scattering processes.*